

# Karbala International Journal of Modern Science

Volume 8 | Issue 3

Article 2

## Performance Simulation for Adaptive Optics Technique Using OOMAO Toolbox

Mahmood Kareem Mirdan

*Department of Astronomy and Space, College of science, University of Baghdad.,  
mahmood.merdan1107@sc.uobaghdad.edu.iq*

Raaid Nawfee Hassan

*Department of Astronomy and Space, College of science, University of Baghdad.*

Bushra Qassim Al-Aboodi

*Department of Astronomy and Space, College of science, University of Baghdad*

Follow this and additional works at: <https://kijoms.uokerbala.edu.iq/home>



Part of the [Computer Sciences Commons](#), and the [Physics Commons](#)

### Recommended Citation

Mirdan, Mahmood Kareem; Hassan, Raaid Nawfee; and Al-Aboodi, Bushra Qassim (2022) "Performance Simulation for Adaptive Optics Technique Using OOMAO Toolbox," *Karbala International Journal of Modern Science*: Vol. 8 : Iss. 3 , Article 2.

Available at: <https://doi.org/10.33640/2405-609X.3233>

This Research Paper is brought to you for free and open access by Karbala International Journal of Modern Science. It has been accepted for inclusion in Karbala International Journal of Modern Science by an authorized editor of Karbala International Journal of Modern Science. For more information, please contact [abdulateef1962@gmail.com](mailto:abdulateef1962@gmail.com).



---

## Performance Simulation for Adaptive Optics Technique Using OOMAO Toolbox

### Abstract

The Adaptive Optics technique has been developed to obtain the correction of atmospheric seeing. The purpose of this study is to use the MATLAB program to investigate the performance of an AO system with the most recent AO simulation tools, Objected-Oriented Matlab Adaptive Optics (OOMAO). This was achieved by studying the variables that impact image quality correction, such as observation wavelength bands, atmospheric parameters, telescope parameters, deformable mirror parameters, wavefront sensor parameters, and noise parameters. The results presented a detailed analysis of the factors that influence the image correction process as well as the impact of the AO components on that process.

### Keywords

Adaptive Optics (AO), OOMAO, Strehl Ratio (SR), Full Turbulence, Residual Turbulence, Noise.

### Creative Commons License



This work is licensed under a [Creative Commons Attribution-NonCommercial-No Derivative Works 4.0 License](https://creativecommons.org/licenses/by-nc-nd/4.0/).

## RESEARCH PAPER

# Performance Simulation for Adaptive Optics Technique Using OOMAO Toolbox

Mahmood K. Mirdan\*, Raaid N. Hassan, Bushra Q. Al-Abudi

Department of Astronomy and Space, College of Science, University of Baghdad, Baghdad, Iraq

### Abstract

The Adaptive Optics technique has been developed to obtain the correction of atmospheric seeing. The purpose of this study is to use the MATLAB program to investigate the performance of an AO system with the most recent AO simulation tools, Objected-Oriented Matlab Adaptive Optics (OOMAO). This was achieved by studying the variables that impact image quality correction, such as observation wavelength bands, atmospheric parameters, telescope parameters, deformable mirror parameters, wavefront sensor parameters, and noise parameters. The results presented a detailed analysis of the factors that influence the image correction process as well as the impact of the AO components on that process.

**Keywords:** Adaptive optics (AO), OOMAO, Strehl ratio (SR), Full turbulence, Residue turbulence, Noise

## 1. Introduction

Adaptive Optics (AO) technology has been utilized for a variety of applications [1]. It aims to capture images with higher resolution or to achieve accurate beam control, which employs a wavefront corrector to regulate and correct the optical wavefront in real-time.

At the height of the cold war, the U.S. department of defense launched a program to develop the first AO system to obtain clearer images of foreign satellites flying overhead. Despite the difficulty, the developments were a huge success and the real-time atmospheric compensator closed the first loop in the laboratory in 1973 [2]. Field experiments will be followed by larger, quicker, and more effective systems, so astronomers have become interested in applying AO to astronomy. Currently, AO technology has been used in astronomical observations [3], retinal imaging [4], laser beam shaping [5], and other fields [6–8].

An AO system, whether used for imaging or laser beam propagation, is made up of three main components that are at the heart of all current AO

systems. These components are the Wavefront Sensor (WFS), the Deformable Mirror (DM), and the Real-Time Computer (RTC) [9]. The majority of the developed systems have a variety of supporting subsystems. These subsystems include the wavefront divider, which is shown in Fig. 1, as a beam splitter and other optical components such as the collecting telescope, imaging optics or scientific camera, and pupil reimaging optics [10].

The configuration of an astronomical AO system is normally set up as illustrated in Fig. 1, where undistorted light beams from a distant reference source travel through the turbulent atmosphere and are absorbed by a telescope. The distorted optical beam is then reduced in diameter [11].

After passing through the wavefront corrector the deformed optical beam is sampled by a beam splitter, which transmits a duplicate of the input wavefront to the WFS. The WFS determines the wavefront departure from a plane wave by measuring the local wavefront slope over an array of subapertures and generating electrical outputs that correspond to the observed optical errors [12]. The data processor, represented by RTC, transforms these error signals into electrical commands, which

---

Received 6 January 2022; revised 7 May 2022; accepted 11 May 2022.  
Available online 1 August 2022

\* Corresponding author:

E-mail addresses: [mahmood.merdan1107@sc.uobaghdad.edu.iq](mailto:mahmood.merdan1107@sc.uobaghdad.edu.iq) (M.K. Mirdan), [raaid.hassan@sc.uobaghdad.edu.iq](mailto:raaid.hassan@sc.uobaghdad.edu.iq) (R.N. Hassan), [bushra.qassim@sc.uobaghdad.edu.iq](mailto:bushra.qassim@sc.uobaghdad.edu.iq) (B.Q. Al-Abudi).

<https://doi.org/10.33640/2405-609X.3233>

2405-609X/© 2022 University of Kerbala. This is an open access article under the CC-BY-NC-ND license (<http://creativecommons.org/licenses/by-nc-nd/4.0/>).

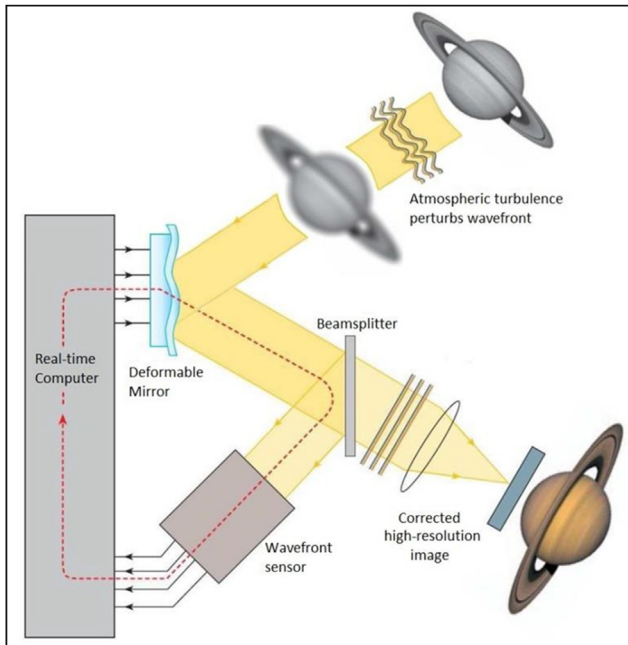


Fig. 1. AO systems arrangement.

are then given back to the wavefront corrector DM. The control loop is closed to a specific number of loop iterations, representing the AO process's recurrence number [13].

## 2. Wavefront representations

The AO system aims to minimize phase aberrations to the absolute minimum to restore image quality in astronomical images. This can be done in two sensing methods: the first is zonal representation, where the wavefront error is described for every point or zone across the pupil. The phase aberration profile in this study is represented using the Zonal method in the form of regular grid surfaces of randomly generated values that follow the Von Karman model of turbulence [14].

An alternative method is model representation. In this approach, a sequence of smoothly varying modes is often used to represent the wavefront surface. These modes might be polynomials or other functions that expand across the telescopes' pupil plane [15,16]. The characterization of the wavefront distortion by decomposing the phase into the Zernike polynomials or modified Zernike polynomials can be found in Refs. [17,18].

### 2.1. Strehl ratio

Several criteria may be used to assess an optical system's performance. However, a parameter that is more commonly used is the Strehl Ratio (SR).

The SR indicates how close the image is to the theoretical diffraction limit, which is the ratio of the maximum intensity of an actual image to the maximum intensity of a fully diffraction-limited image normalized to have the same total flux [19].

The SR of an image is determined by the variance of the pupil phase, as follows [20]:

$$SR \cong \exp(-\sigma_\phi^2) \quad (1)$$

where  $\sigma_\phi^2$  represents the variance of the phase  $\phi$  measured in ( $\text{rad}^2$ ). It's clear for a pupil of any shape that the SR for small aberrations is determined by its variation throughout the apodized pupil rather than its type.

The SR value is always between 0 and 1, and in a real optical system, it is impossible to obtain an SR of unity, where the aberrations and amplitude variations in the pupil (for example, an annular aperture) always reduce the SR [21].

### 2.2. Simulation toolbox

Simulation is essential for the development of any AO system since it allows designers to set the parameters of the AO components, troubleshoot the system, and even evaluate the efficiency of a system on a specific instrument.

Some of the modeling tools are Code for Adaptive Optics Systems (CAOS), which is a software application that allows a quick study of all the modules in a conventional AO system [22]. A second tool is Yao, which stands for Yorick Adaptive Optics, which is an open-source AO software simulation package that is used to simulate medium-size AO systems for extremely large telescopes [23]. It is fast, flexible, and an open-source library on Github [24], where installation is supported on Linux and OsX.

In this paper, Objected-Oriented Matlab Adaptive Optics (OOMAO) has been utilized, which is a Matlab toolbox and the most recent AO modeling tool developed by Conan and Correia (2014) to model an entire AO system [25]. OOMAO is designed fully in the Matlab programming language and employs various Matlab-built algorithms that have been written and optimized in packages of code. OOMAO's Matlab source code is freely available to download on the Github website [26].

As the title implies, the package was designed in an object-oriented style. Object-Oriented Programming, or OOP, is a contemporary programming language that allows for the easy and manageable building of huge and complex software architectures. OOP is a programming paradigm that focuses on objects and data rather than actions and logic [27].

OOMAO was built on a combination of classes that represent the atmosphere, source, telescope, DM, WFS, and an imager of the AO system. This basic set of classes enables the modeling of Natural Guide Star (NGS), Laser Guide Star (LGS), Single Conjugate Adaptive Optics (SCAO), and Laser Tomography Adaptive Optics (LTAO) systems on telescopes as large as extremely large telescopes. OOMAO has its own dynamic influence function model for simulating various types of DMs, LGSs' cone effect, altitude thickness, and intensity profile are emulated as well. Modal and zonal modeling approaches are both implemented. OOMAO also contains a large theoretical expression library for evaluating the statistical features of turbulence wavefronts.

### 3. Results and discussion

The simulation outputs of OOMAO have been analyzed in general and OOMAO's class parameters in particular. The analysis was carried out by studying the image quality metrics and how they were affected by the parameter changes.

In this study, the image quality metrics were confined to SR, which is calculated by the empirical expression in equation (1). SR is computed from the phase variance of the aberrated wavefront and the wavefront after the compensation. This process is completed in two cases, with and without WFS detector read-out noise.

Overall, the calculation outcomes will be four vector rows for SR, where the phase of the aberrated wavefront is referred to as “Full Turbulent” and the phase of the compensated wavefront is referred to as “Residue Turbulent.” While in the noise case, the term “noise” is added to the labels (i.e., Full Turbulent means AO off and Residue Turbulent means AO on) it is good to mention that higher SR is desired.

In this work, analysis of parameters variation included the NGS's observed wavelength bands regarding source class, the Fried coherence parameters  $r_0$  and time constant  $\tau_0$  regarding atmosphere class, the telescope aperture diameter regarding telescope class, the number of DM's actuators and actuator mechanical coupling regarding DM class, the number of lenslets array regarding Shack-Hartmann Wavefront Sensor (SH-WFS) class, and finally the noise effect.

#### 3.1. SR criteria of the observed bands

Several wavelength bands of observed NGSs have been analyzed as shown in Table 1. OOMAO is

Table 1. NGS's observed wavelength bands.

Spectrum	Band	Wavelength ( $\mu\text{m}$ )
Visible	B	440
	V	500
	R	640
Infrared	I	790
	J	1215
	H	1654
	K	2179

\*Special description of the title. (dispensable).

equipped with a set of photometric bands within the photometry object. These band sets were plotted against the SR of the aberrated and compensated wavefront, as shown in Fig. 2.

To view the relationship between the AO correction ability and the photometric bands, the SR was plotted as a function of the observed wavelengths, as illustrated in Fig. 3.

The results in Figs. 2 and 3 were obtained using a circular aperture with a telescope aperture diameter of 3.6 m. The same atmospheric layers for each wavelength were used with Fried coherence parameters  $r_0 = 15$  cm, the lenslets array is  $10^2$ , 50% DM's actuator coupling, and for 400 loop iterations with detector read-out noise of about 5 photo-electron/pixel/frame.

It's clear that from Figs. 2 and 3, the correction processes (compensations) are proportional to longer wavelengths and high bands. Whereas they head toward higher wavelengths, they are less affected by atmospheric turbulence.

#### 3.2. Fried parameter, time constant and seeing

The most important parameters in the AO field are the Fried Coherence Length  $r_0$  and atmospheric time constant  $\tau_0$ , which have been analyzed. Fried's parameter is a widely used descriptor of the level of atmospheric turbulence at a particular site, while the atmospheric time constant is the rate of change in wavefront phase structure; this is due primarily to the wind that carries the turbulence pattern as it passes over the telescope.

SR was plotted as a function of the Fried coherence length  $r_0$  in cm and atmospheric time constant  $\tau_0$  in milliseconds, as shown in Fig. 4, computed for NGS at J-band with three identified atmospheric layers, a 3.6 m telescope aperture diameter and a  $10^2$  lenslet array of SH-WFS.

The results in Fig. 4, demonstrate that the SR of the correction process has the same behavior as the SR of the observed bands when compared to Fig. 3. This returns to the proportional relationship in the atmospheric structure-function equation between

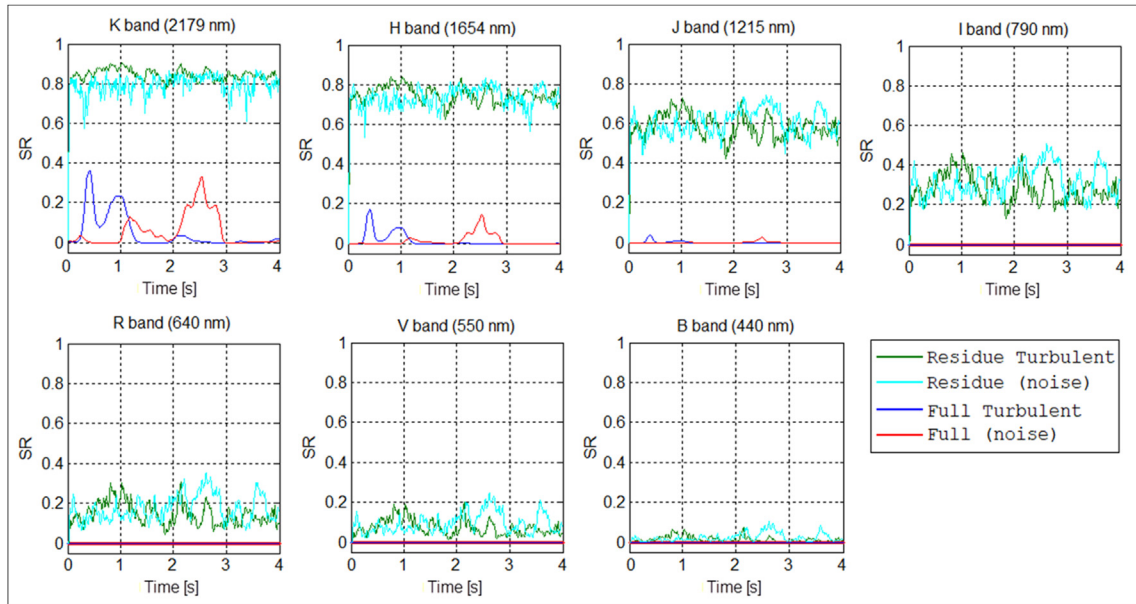


Fig. 2. SR as a function of the observed wavelength bands.

the Fried coherence length and wavelength, where  $r_0 \propto \lambda^{6/5} \Rightarrow SR \propto \lambda \alpha r_0$ .

Further, the SR has another proportional relationship which is that with  $\tau_0$ , since  $\tau_0$  has proportionality with  $r_0$  as  $\tau_0 = 0.314 r_0 / v$  ( $v$  stands for wind speed),  $\tau_0 \alpha r_0 \Rightarrow SR \alpha r_0 \alpha \tau_0$  this explains the SR increment with time constant rate. The importance of  $\tau_0$  calculations to an AO system is to determine the Greenwood frequency of that system, which gives an idea of how fast the AO system must respond to the phase structure changes.

Also in Fig. 4, shows the strength of the turbulence effects on the seeing disk (seeing is a term used to illustrate how light entering a telescope can change direction randomly), where the small values of  $r_0$  and  $\tau_0$  correspond to strong turbulence (poor seeing), while large values correspond to weak

turbulence (good seeing). This highly depends on the observation location.

For a deep investigation of the seeing effect, it's plotted versus SR, as shown in Fig. 5. It is clear that a bit of change in seeing disk caused a high incline in the SR. This in turn caused a blurring in image quality. That's due to the inverse proportional of seeing  $\epsilon$  with Fried parameter as  $\epsilon = 0.98 \lambda / r_0$  where  $\epsilon \propto r_0^{-1}$ .

### 3.3. Telescope aperture diameter

The telescope aperture diameter has been analyzed and several circular aperture diameters in meters are plotted versus SR, as shown in Fig. 6.

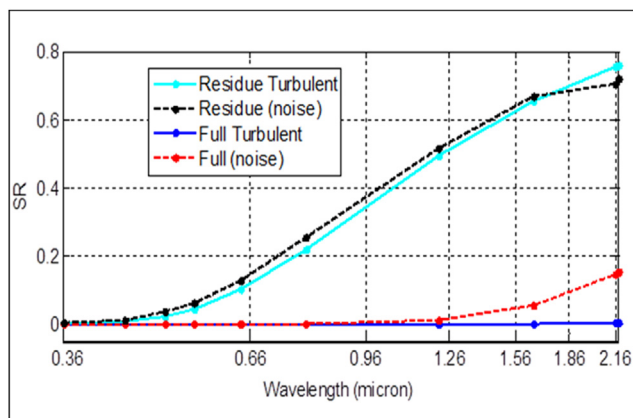


Fig. 3. SR as a function observed wavelengths.

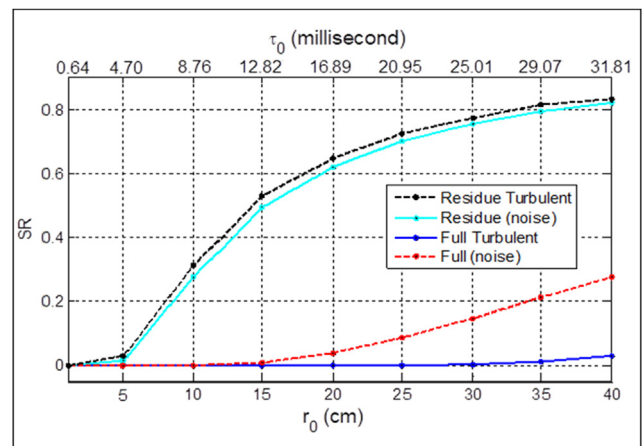


Fig. 4. Fried Coherence Length and Time Constant vs. SR.

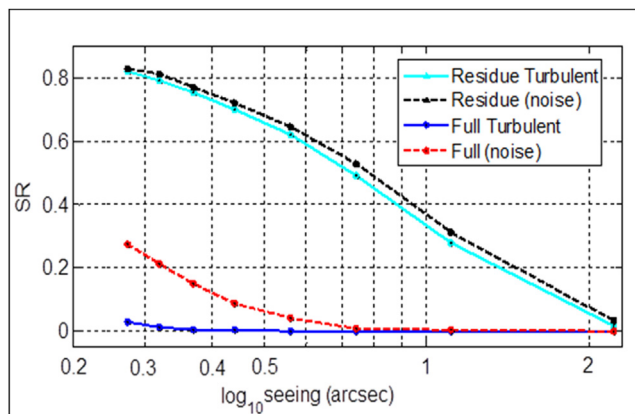


Fig. 5. The performance of AO system with seeing effect.

This was carried out by a constant DM actuator density across all tested apertures.

The results clearly show the inverse relationship between SR and aperture diameter, so that when the telescope aperture is increased by 1 m, the SR decreases by an average of about 17%.

The distinction here is that in the noise case at 1 m aperture diameter, SR has the same value as the full aberrated and compensated phase. This is the reason that the AO system is built for telescopes with 3 m apertures or bigger.

### 3.4. Shack-Hartmann Wavefront Sensor lenslet arrays

The phase recovery at subapertures of SH-WFS lenslets has been analyzed and plotted against SR as illustrated in Fig. 7, which also represents the analysis of the number of actuators of DM since it correlates to the lenslet arrays according to Fried geometry. The analysis was performed for NGS at J-band,  $D = 3.6$  m,  $r_0 = 15$ , and actuator coupling of 50%.

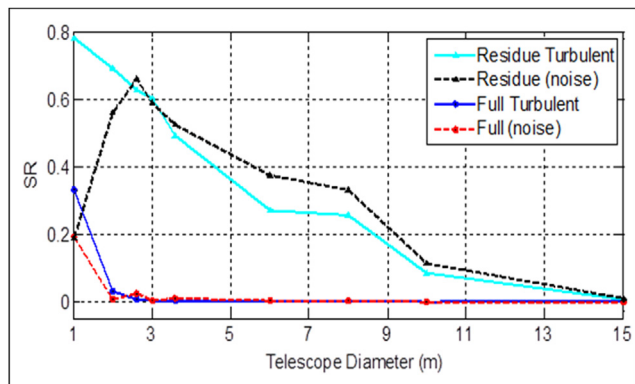


Fig. 6. The performance of AO system with telescope aperture diameter.

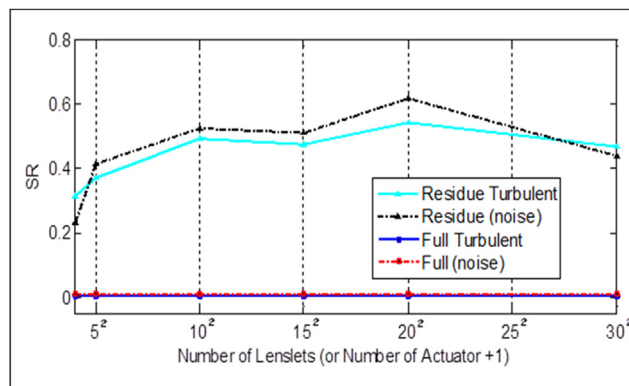


Fig. 7. The performance of AO system with lenslets array size (or actuator array size +1).

The results showed that the best lenslet array size for an aperture diameter of  $D = 3.6$  m is a  $20 \times 20$  subaperture array.

### 3.5. DM's mechanical coupling

The DM actuators' mechanical coupling has been analyzed and plotted versus SR as shown in Fig. 8, and it was calculated for NGS at J-band,  $D = 3.6$  m,  $r_0 = 15$  cm.

The coupling parameter in percentage is linked to DM's influence function that gives DM the shape. This parameter shows how much the movement of one actuator will displace its neighbors. The analysis showed that actuators with high mechanical coupling ( $>50\%$ ) reduce the compensation efficiency by 25% and even get worse at very high values. As is obvious in Fig. 8, for a full mechanical coupling (90–100% actuator coupling) the performance indicator was extremely dropped because of the inability of DM to produce the required compensations.

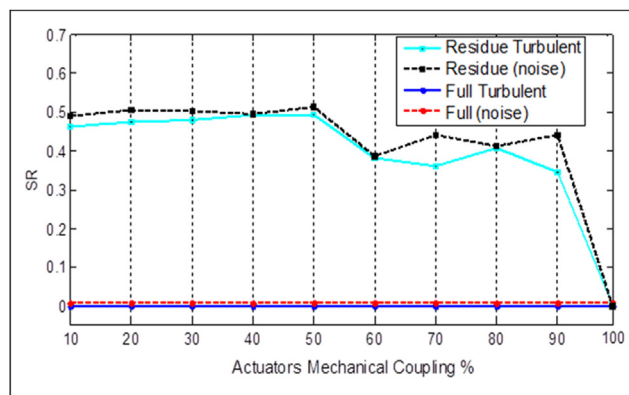


Fig. 8. The performance of AO system with actuators mechanical coupling.

### 3.6. Detector read-out noise

The read-out noise of the SH-WFS detector is investigated and analyzed. It's determined for NGS at J-band with an apparent magnitude of 10,  $D = 3.6$  m,  $r_0 = 15$  cm, and a lenslet array of SH-WFS  $10^2$  with a closed-loop number of iterations of 20. The measuring unit of this type of noise is photo-electron per pixel root mean square (rms) per frame, which means that every pixel in every taken frame has the same read-out rms noise characteristics (with the exception of some edge pixels).

Every optical instrument is influenced by noise. Since the telescopes observe very faint objects, the noise may cover the observed signal. In this work, the effect of detector noise shows how noise degrades the wavefront measurements, leading to degradation in AO performance. But when plotted against SR (see Fig. 9) and compared with noiseless residue turbulent, it's found that at lower noise levels the read-out noise causes a bit of a raise in the wavefront phase compensation until reaching a specific threshold (here at 9 photo-electron) and above, the noise effect takes its turn in degrading the compensation process.

This is possibly due to the low time duration throughout the compensation (closed-loop iterations number). This can be confirmed by comparison with Fig. 2, the J-band subplot, where the difference between the mean of the noiseless residue turbulent and the noisy one at (5 photo-electron detector noise) is about 0.0320 for 20 loop iterations, while for 400 loop iterations the difference is about 0.0185.

### 3.7. Photon background noise

The photon background or sky background noise has been analyzed and determined to be the same set-up as the read-out noise detection for NGS with an apparent magnitude of 10. The measuring unit of

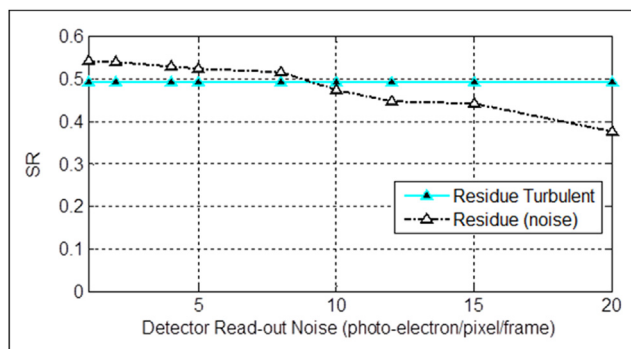


Fig. 9. Detector Read-out Noise vs. SR.

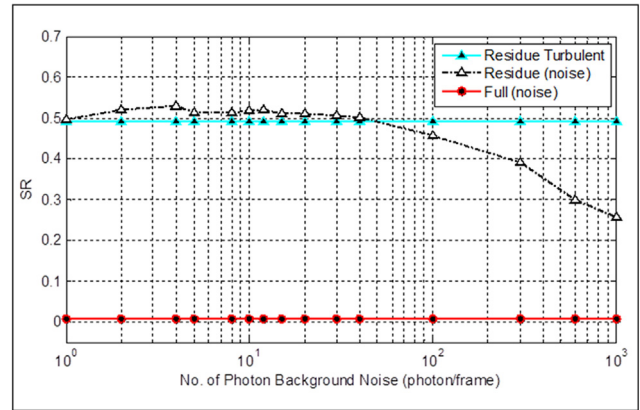


Fig. 10. Photon Background Noise vs. SR.

this noise is photons per frame, which means the detected number of photons is for the whole taken frame.

As with read-out noise, the photon noise also raised the values of the wavefront phase compensation, but at a lower rate than the read-out noise, as shown in Fig. 10, when plotting SR as a function of photon background.

On the other hand, the degradation in performance begins after the threshold (at 50 photons per frame). Although both sensed noises have the same affection behavior on AO performance, the photon noise has a higher impact ratio compared to the read-out noise.

This was done by comparing noises at a specific value with the noiseless SR residue turbulent. The results showed that read-out noise reduces the compensation process by 10% and photon background noise reduces it by 40%.

## 4. Conclusion

This work investigated a statistical analysis of the physical performance of an AO system; our conclusions can be summarized by the following main points:

- The performance of an AO system is highly affected by the observed wavelength, so for good image quality it's better for a single conjugate adaptive optics system to observe near-infrared wavelengths or higher.
- The atmospheric parameters are important for the observing process since the strength of the atmospheric turbulence and seeing conditions negatively affect the image quality. So to get the best astronomical observations, the site selection (high altitude locations) and the seeing conditions ( $r_0 > 15$  cm) must be kept in mind.

- In general, AO systems are built for large telescopes, and this work demonstrated the inverse relationship between AO performance and aperture diameter. So when the telescope aperture is increased by 1 m, the performance decreases by an average of about 17%. Thus every large telescope (>3 m) has special and appropriate AO system configurations in order to get the best results from the attached system.
- The number of DM's actuators is correlated with the number of SH-WFS lenslets array, and for the best phase recovery and compensation, each telescope aperture has a specific lenslet array size that is appropriate to the aperture shape and diameter. Further, the low mechanical coupling between neighboring actuators of DMs improves AO system performance.
- The noise effect (detector read-out noise and photon background noise) on the AO system may have the same affection behavior on AO performance but different degradation values, where the photon background noise degrades AO performance by 30% more than the detector read-out noise.
- Finally, for a specific telescope the OOMAO toolbox can be used to get the best AO system configuration, which will grant the highest observing performance and image resolution.

## 5. Recommendations

We recommend that large telescopes (>3 m) operate at infrared wavelengths, especially in poor seeing conditions. Also minimize the DM's actuator coupling and WFS noise as much as possible.

## Acknowledgements

The authors would like to thank the editors and the anonymous reviewers for their valuable comments and suggestions, which have helped immensely in improving the quality of the paper.

## References

- [1] H. Babcock, The possibility of compensating astronomical seeing, *Astron Soc Pacif.* 65 (1953) 229–236.
- [2] F. Rigaut, B. Neichel, Multiconjugate adaptive optics for astronomy, *Annu Rev Astron Astrophys.* 56 (2018) 277–314, <https://doi.org/10.1146/annurev-astro-091916-055320>.
- [3] R. Davies, M. Kasper, Adaptive optics for astronomy, *Annu Rev Astron Astrophys.* 50 (2012) 305–351, <https://doi.org/10.1146/annurev-astro-081811-125447>.
- [4] S. Niu, J. Shen, C. Liang, Y. Zhang, B. Li, High-resolution retinal imaging with micro adaptive optics system, *Appl Opt.* 50 (2011) 4365–4375, <https://doi.org/10.1364/AO.50.004365>.
- [5] H. Ma, Z. Liu, X. Xu, J. Chen, Simultaneous adaptive control of dual deformable mirrors for full-field beam shaping with the improved stochastic parallel gradient descent algorithm, *Opt Lett.* 38 (2013) 326–328, <https://doi.org/10.1364/OL.38.000326>.
- [6] R. Bastaitis, D. Alaluf, M. Horodincă, I. Romanescu, I. Burda, G. Martic, G. Rodrigues, A. Preumont, Segmented bimorph mirrors for adaptive optics: segment design and experiment, *Appl Opt.* 53 (2014) 6635–6642, <https://doi.org/10.1364/AO.53.006635>.
- [7] A. Bayanna, R. Louis, S. Chatterjee, S. Mathew, P. Venkatakrisnan, Membrane-based deformable mirror: intrinsic aberrations and alignment issues, *Appl Opt.* 54 (2015) 1727–1736, <https://doi.org/10.1364/AO.54.001727>.
- [8] H. Ma, P. Zhou, X. Wang, Y. Ma, F. Xi, X. Xu, Z. Liu, Near-diffraction-limited annular flattop beam shaping with dual phase only liquid crystal spatial light modulators, *Opt Express.* 18 (2010) 8251–8260, <https://doi.org/10.1364/OE.18.008251>.
- [9] R. Tyson, Principles of adaptive optics, third ed., CRC Press, Florida, 2010.
- [10] R. Tyson, Introduction to adaptive optics, first ed., SPIE Press, Washington, 2000.
- [11] R. Parenti, Adaptive optics for astronomy, *Linc Lab J.* 6 (1992) 92–114.
- [12] J. Hardy, Adaptive optics for astronomical telescopes, first ed., Oxford University Press, New York, 1998.
- [13] R. González-Acuña, H. Chaparro-Romo, General mirror formula for adaptive optics, *Appl Opt.* 60 (2021) 375–379, <https://doi.org/10.1364/AO.413940>.
- [14] T. Von Karman, Progress in the statistical theory of turbulence, *Proc Natl Acad Sci Unit States Am.* 34 (1948) 530–539.
- [15] W. Southwell, Wave-front estimation from wave-front slope measurements, *J Opt Soc Am.* 70 (1980) 998–1006, <https://doi.org/10.1364/JOSA.70.000998>.
- [16] M. Chebbo, Simulation fine D'optique adaptative A tres grand champ pour des grands et futurs tres grands telescopes, doctoral dissertation, Aix Marseille University, 2012.
- [17] L. Abood, S. Al-Hilly, R. Hassan, Describing the wavefront aberrations of the hexagonal aperture using modified Zernike polynomials, *Iraqi J Sci.* 54 (2013) 222–231.
- [18] W. Wadee, R. Hassan, Effect of the static aberration on the extended objects, *Iraqi J Sci Spec Issue.* (2016) 215–224. Part A.
- [19] Z. Wu, A. Iqbal, F. Ben Amara, Modeling and control of magnetic fluid deformable mirrors for adaptive optics systems, first ed., Springer, New York, 2013 <https://doi.org/10.1007/978-3-642-32229-7>.
- [20] T. Ross, Limitations and applicability of the Maréchal approximation, *Appl Opt.* 48 (2009) 1812–1818, <https://doi.org/10.1364/AO.48.001812>.
- [21] W. Leung, Inverse problems in astronomical and general imaging, Doctoral dissertation, University of Canterbury, 2002.
- [22] M. Carillet, C. Verinaud, M. Guarracino, L. Fini, O. Lardiere, B. Le Roux, A.T. Puglisi, B. Femenia, A. Riccardi, B. Anconelli, S. Correia, M. Bertero, P. Boccacci, CAOS: a numerical simulation tool for astronomical adaptive optics (and beyond), *Proc SPIE.* 5490 (2004) 637–648, <https://doi.org/10.1117/12.551552>.
- [23] F. Rigaut, M. van Dam, Simulating astronomical adaptive optics systems using Yao, in: Proceedings of the third AO4ELT conference, 2013.
- [24] F. Rigaut, M. van Dam, J. Cranney, S. Hippler, Yao an adaptive optics simulation package. <http://github.com/frigaut/yao>. (Accessed 3 January 2022).
- [25] R. Conan, C. Correia, Object-oriented Matlab adaptive optics toolbox, *Proc SPIE.* 9148 (2014) 1–17, <https://doi.org/10.1117/12.2054470>.
- [26] R. Conan, Object-oriented Matlab adaptive optics. <https://github.com/rconan/OOMAO>. (Accessed 3 January 2022).
- [27] A. Reeves, Laser Guide star only adaptive optics: the development of tools and algorithms for the determination of laser Guide star tip-tilt, doctoral dissertation, Durham University, 2015.